Astron. Astrophys. 353, 322–334 (2000)

ASTRONOMY AND ASTROPHYSICS

Optical and near-infrared spectrophotometric properties of Long Period Variables and other luminous red stars

R. Alvarez[1], **A. Lançon**[2], **B. Plez**[3], **and P.R. Wood**[4]

[1] IAA, Université Libre de Bruxelles, C.P. 226, Bvd du Triomphe, 1050 Bruxelles, Belgium (ralvarez@astro.ulb.ac.be)
[2] Observatoire de Strasbourg, UMR 7550, 11 Rue de l'Université, 67000 Strasbourg, France (lancon@astro.u-strasbg.fr)
[3] GRAAL, Université Montpellier II, cc072, 34095 Montpellier cedex 05, France (plez@graal.univ-montp2.fr)
[4] RSAA (ANU), Mount Stromlo Observatory, Private Bag, Weston Creek, ACT 2611, Australia (wood@mso.anu.edu.au)

Received 6 August 1999 / Accepted 29 October 1999

Abstract. Based on a new and large sample of optical and near-infrared spectra obtained at the Mount Stromlo and Siding Spring Observatories (Lançon & Wood 1998; Lançon & Wood, in preparation), spectrophotometric properties of cool oxygen- and carbon-rich Long Period Variables and supergiants are presented. Temperatures of oxygen-rich stars are assigned by comparison with synthetic spectra computed from up-to-date oxygen-rich model atmosphere grids. The existence of reliable optical and near-infrared temperature indicators is investigated. A narrow relation between the bolometric correction BC_I and the broad-band colour I−J is obtained for oxygen-rich cool stars. The ability of specific near-infrared indices to separate luminosity classes, atmospheric chemistry or variability subtypes is discussed. Some comments are also given on extinction effects, water band strengths in Long Period Variables and the evaluation of $^{12}CO/^{13}CO$ ratio in red giants.

Key words: stars: AGB and post-AGB – stars: carbon – stars: fundamental parameters – stars: late-type – stars: oscillations

1. Introduction

The near-infrared (NIR) radiation of our and other galaxies is essentially provided by luminous red stars: red supergiants dominate in starburst regions, Asymptotic Giant Branch stars (AGBs), among which the O-rich and C-rich Long Period Variables (LPVs) of various variability types, take over in stellar populations with ages between 10^8 and 10^9 years, and First Giant Branch stars dominate in older regions (Bruzual & Charlot 1993; Lançon 1999). In view of the recent developments in NIR observational technology, tools have become necessary that would allow us to connect NIR spectrophotometric signatures with the fundamental stellar properties provided by theoretical stellar evolution tracks. Only then can integrated NIR emission properties or star counts be interpreted in terms of galaxy history. These connection tools are also needed from a purely stellar perspective. The evolution, structure and atmospheres of the evolved red stars are among the standing problems in stellar astrophysics and valuable constraints on the models are to be expected from population studies. The choice of suitable filter passbands, able to separate stellar subtypes, is a prerequisite for efficient surveys.

In this paper, the emphasis is set on LPVs, which constitute the most luminous and coolest but also the most complex population of red giants in regions where more massive red supergiants have died. Static red giant model atmospheres are progressing rapidly due to recent improvements in molecular opacity data (Plez 1999a, 1999b). Variable star models are still far from satisfactory because of the interplay between pulsation, radiative transfer and chemistry (see Höfner 1999 for a review). Empirical spectroscopic or spectrophotometric studies adequate for our purpose have remained scarce because they are time consuming and because a significant wavelength coverage requires synchronised observations: LPV periods are typically one year long and cycle to cycle variations common. In addition, since good infrared instrumentation is usually found on relatively large telescopes that tend to be preferentially directed towards faint sources instead of bright stars, most previous photometric studies of LPVs have been optical (Kerschbaum & Hron 1996; Alvarez & Mennessier 1997; Wing et al. 1998). Based on a new, rich sample of complete optical+NIR spectra of red stars, we are able to extend these studies.

The properties of the data are summarised in Sect. 2. In Sect. 3, we discuss spectrophotometric temperature indicators at optical and NIR wavelengths. The physical significance and absolute calibration of the empirical scales, in particular for variable stars, will be discussed in more depth elsewhere. The subsequent sections discuss the ability of commonly used and newly defined NIR narrow band indices to separate luminosity, surface chemistry or variability subtypes. The results are summarised in Sect. 10.

2. The sample

The reader is referred to Lançon & Wood (1998) and Lançon & Wood, in preparation, for a thorough description of the sample. Around one hundred spectra of cool stars ranging from 5100 Å

Send offprint requests to: R. Alvarez
Correspondence to: ralvarez@astro.ulb.ac.be

to 2.5 μm have been obtained at the Mount Stromlo and Siding Spring Observatories, using the three cross-dispersed grisms of CASPIR[1] on the 2.3 m Telescope (near-infrared spectra with a resolution R of 1100) and a low resolution grating spectrograph on the 74 inch Telescope (optical spectra, R $\simeq$ 30). The sample mainly contains instantaneous spectra of O-rich and C-rich local LPVs[2], but also includes local non-variable giants and a few luminous LPVs from the Magellanic Clouds and the Galactic Bulge. Additional spectra restricted to either the optical (5100–9900 Å) or the NIR region (9750–24900 Å) are available for some stars and are included in the analysis whenever possible.

3. Temperature indicators

3.1. Temperature definitions

Only little is known about effective temperatures of LPVs. In principle, the effective temperature relates the bolometric luminosity of a star to its effective radius and is thus accessible through surface brightness measurements, i.e. apparent luminosities combined with angular diameters (e.g. Perrin et al. 1998). However, due to their very extended atmospheres, LPVs such as Miras cannot easily be assigned a unique radius: observational determinations are wavelength dependent and depend on the adopted limb-darkening law (Labeyrie et al. 1977; Baschek et al. 1991; Hofmann et al. 1998). The use of model atmospheres is inevitable not only in providing these laws in the various observational filter passbands, but also to relate the resulting "monochromatic" radii to the effective radius (usually based on Rosseland mean optical depths) that is used in the effective temperature definition of stellar models. Large uncertainties and inconsistencies between authors occur as a result of e.g. incomplete treatment of molecular opacities in the models, of different assumptions on the stellar pulsation mode or on whether or not the phase in the pulsation cycle is taken into account (Scholz & Takeda 1987; Haniff et al. 1995; van Belle et al. 1996; Bessell et al. 1996).

Photometric indices, i.e. colours and molecular band strength measurements, provide alternative effective temperature estimates (Ramírez et al. 1997; Alvarez & Mennessier 1997). Optical indices define the spectral types, which are calibrated against the effective temperature either on the basis of angular diameter measurements (Ridgway et al. 1980; Perrin et al. 1998) or by direct comparison with synthetic spectra (Fluks et al. 1994). The calibrations inherit the model dependence already mentioned. In addition they generally assume a unique relation between spectral type and effective temperature, independent of variability type or time. This assumption oversimplifies the real situation: Alvarez & Plez (1998) have shown that TiO and VO bands, two temperature sensitive indicators, do not vary in phase along the Mira luminosity cycle, and the data used here contains pairs of spectra with insignificant differences below 1 μm but very different NIR H_2O vapour bands. As expected from the complex stratification of dynamical atmosphere models (Bowen 1988; Fleischer et al. 1992; Höfner et al. 1998) molecular indices contain local information and are sensitive each in its own way to the details of the pulsation history as well as to the global property called effective temperature.

In view of the above difficulties, this paper avoids direct comparison with dynamical model atmospheres. A temperature refered to as the *"static" effective temperature* (and noted $T_{\rm eff}$ throughout the paper for simplicity)[3] is nevertheless tentatively assigned to each spectrum, based on the fact that the optical part of the static and variable giant spectra in our sample can indeed be reasonably well fitted with static giant models. The resulting absolute $T_{\rm eff}$ scales may be biased estimates of the real effective temperatures, but a better understanding of pulsating models is required before these biases can be evaluated and their dependence on the pulsation properties accounted for. The static $T_{\rm eff}$ scale is used to calibrate photometric temperature scales and all further discussion then relies on purely empirical findings.

3.2. Static effective temperature assignment

The synthetic spectra used for the static $T_{\rm eff}$ assignment are computed from a large grid of MARCS models (Plez et al. 1992; Plez 1992; Plez, private communication) representing red giants with solar composition and different values of atmospheric extension, surface gravities $\log g$ ranging from -0.5 to 3.5, and of effective temperatures from 2400 to 4750 K. The spectral synthesis includes the updated opacity data for TiO (Plez 1998), VO and H_2O as detailed in Bessell et al. (1998) and Alvarez & Plez (1998). The latest models are preliminary computations of a large new and updated grid now being computed by the Uppsala group.

The static $T_{\rm eff}$ associated with a spectrum is defined here as the effective temperature of the MARCS model that provides the minimum χ^2 fit to the 5100–9950 Å data, $\log g$ and atmospheric extension being allowed to vary freely.

We have determined this $T_{\rm eff}$ for 131 spectra of oxygen-rich giants, among which some are Mira, Semi-Regular (SRa and SRb types) or Irregular variables, observed at various phases. The sensitivity of the spectra to $T_{\rm eff}$ combined with the step of the model grid allows us to assign $T_{\rm eff}$ values to $\pm$100 K (cf. Fig. 1). The corresponding acceptable $\log g$ values lie between 0.0 and 1.5, a range over which spectral variations are much smaller than those produced by a 100 K change in $T_{\rm eff}$.

3.3. Photometric temperature indicators

The following sections discuss narrow band and broad band colours derived from the observed spectra. We use filters similar to those of Wing (1967) and White & Wing (1978), adopting the passbands defined by Bessell et al. (1989a); we complete the set with filters from Fluks et al. (1994) and additional indices designed to measure OH, H_2O and CO band strengths. The

[1] Cryogenic Array Spectrometer and Imager, McGregor 1994

[2] All variability types used in this paper are from the *General Catalogue of Variable Stars* (Kholopov et al. 1988)

[3] "Effective temperature", *in extenso*, is used when the theoretical quantity is meant.

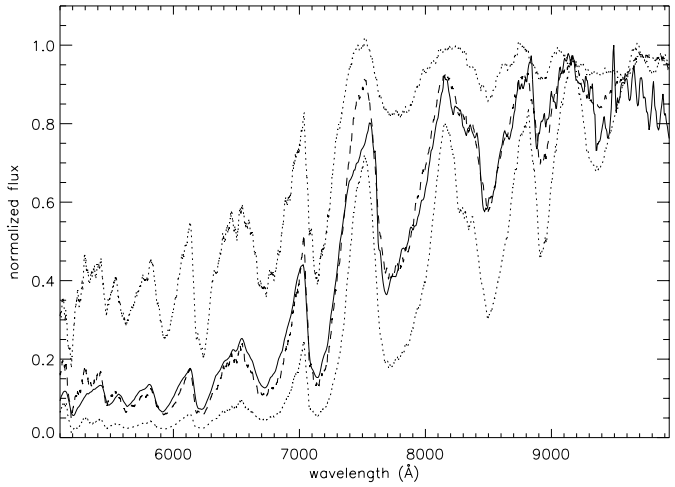

Fig. 1. Observed spectrum of S Phe, a M6 SRb variable (full line) and synthetic spectrum with $T_{\rm eff}$=3400 K, $\log g$=1.0 and $\mathcal{M}$=1.0 $\mathcal{M}_{\odot}$ (dashed line). The dotted lines are two synthetic spectra with $T_{\rm eff}$=3200 K and 3600 K

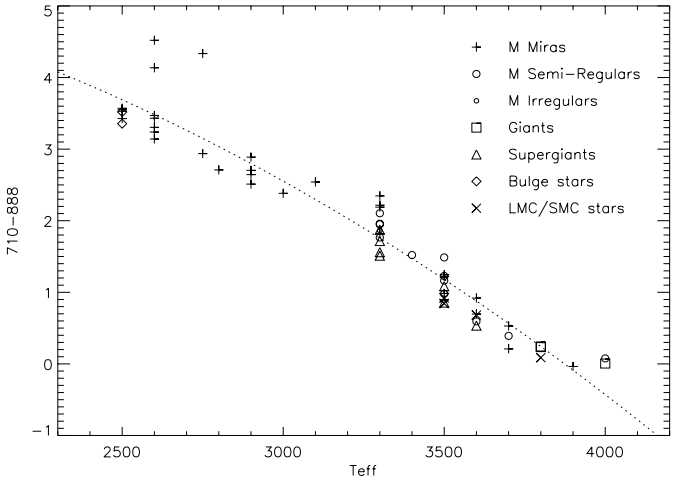

Fig. 2. The 710−888 index as a function of the effective temperature derived from the fit of MARCS models to the optical spectrum (plus signs: M Miras; empty circles: M Semi-Regulars; small empty circles: M Irregulars; squares: K and M giants; triangles: supergiants; diamonds: bulge stars; crosses (X): LMC/SMC stars)

VRIJHK colours are computed with the passbands of Bessell & Brett (1988) and Bessell (1990). The zero point calibrations are based on a spectrum of Vega (Castelli & Kurucz 1994) as used by Bessell et al. (1998): the colours of Vega are set equal to zero, except for the Wing colours for which we used Vega's observed colours (Wing, private communication).

3.3.1. Optical temperature indicators

Most optical colours appear to be quite good temperature indicators (e.g. 710−888, 847−839, 710−745, 888−883 as used by Wing, or $S_{1/2,Sp}$, $S_{2/3,Sp}$ as in Fluks et al. 1994).

Fig. 2 shows the 710−888 index as a function of the $T_{\rm eff}$ assigned previously. This index has been chosen to be our temperature indicator subsequently as its scale of variation is large and the scatter is small. It measures the ratio between the bandheads of the TiO γ Δv=0 and the TiO δ Δv=0 ro-vibrational transitions (Brett 1990). The 710 and 888 filters are displayed on Fig. 3. A least-square polynomial fit gives:

$$(710\text{–}888) = 5.8 + 3.2\,10^{-4} \times T_{\rm eff} - 4.7\,10^{-7} \times T_{\rm eff}^2 \qquad (1)$$

The standard deviation is 0.3 mag in the range 2500 K $\leq T_{\rm eff} \leq$ 3900 K.

It is worth noticing that non-variable and variable stars on one hand, local, Bulge and LMC/SMC stars on the other hand, all seem to follow the same relation. This may be surprising at first thought. In fact, it shows that the relation between the 710−888 index and the whole optical spectrum used in our χ^2 adjustment doesn't depend strongly on metallicity or variability type. The optical parts of the spectra all tend to lie on a tight sequence (which makes the fits with static model spectra possible). It doesn't imply, however, that the effective temperature scale along this sequence is independent of the object type or metallicity: our $T_{\rm eff}$ assignment based on the optical spectrum is liable to be a good estimate of the real effective temperature of static stars, but could be systematically different from the effective temperature in variable objects.

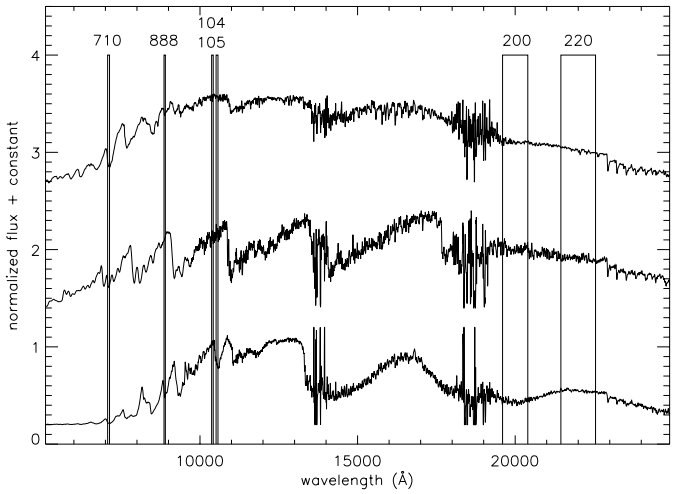

Fig. 3. Narrow-band filters used in Sect. 3. The spectra are from bottom to top: R Phe, a O-rich Mira; RU Pup, a C-rich Semi-Regular and HD 101712, a supergiant. Regions around 1.4 and 1.9 μm are associated with extreme telluric water absorption

Only two Bulge stars of our sample were observed in the optical region. More observations are required to make firm statements on their specific static $T_{\rm eff}$ versus (710−888) relation.

The outlying points in Fig. 2 at 710−888 $\geq$ 4 are three observations of SV Lib, a M8 Mira star. These values of the TiO index would lead to particularly low temperatures when extrapolating the $T_{\rm eff}$–(710−888) relation without caution. However, the global energy distribution of the star and the discussion in the following section argue against such an interpretation. These points were not taken into account when deriving Eq. (1).

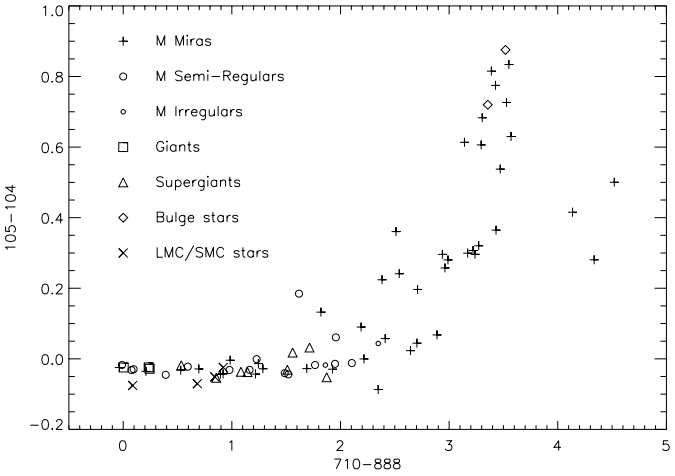

Fig. 4. The 105−104 index versus the $T_{\rm eff}$ indicator 710−888

3.3.2. Near-infrared temperature indicators

For extragalactic study purposes, near-infrared temperature indicators are of great interest. Indeed, the contribution of AGB stars to the emission of a stellar population is largest in this spectral range, and the population synthesis predictions are thus particularly sensitive to temperature–colour–spectral feature relations (Lançon 1999).

We have applied various near-infrared filters to the observed spectra. In Fig. 4, the Wing VO index 105−104 is plotted against our optical $T_{\rm eff}$ indicator 710−888. There is a good correlation between the two colours, the VO index becoming a useful $T_{\rm eff}$ index below 3300 K, as already found by Bessell et al. (1989a) from synthetic spectra. The 104 and 105 filters are shown in Fig. 3. The scatter of Fig. 4 might be due to atmospheric extension, surface gravity or metal abundance (Bessell et al. 1989a) but the main source of scatter is certainly variability, Miras executing loops in such TiO/VO diagrams (Bessell et al. 1996; Alvarez & Plez 1998).

The three outlying points (710−888≥4) are, again, the observations of SV Lib. This M8 Mira star has strong TiO absorption at 710 nm but normal VO bands (see also Lançon & Wood 1998). The observations were taken at different dates: the effect cannot be associated with errors in the acquisition or the reduction of the data. This star deserves further scrutiny and in particular a more complete phase coverage to clarify its peculiarities.

It is difficult to define near-infrared colours more convenient than 105−104 that might be used as $T_{\rm eff}$ indicators. The CO (2.3 μm) equivalent width suggested by Ramírez et al. (1997) appears inadequate: the correlation with $T_{\rm eff}$ is only marginally significant in our LPV sample. The large dispersion is mainly due to variations of the order of 10 Å in the CO equivalent width of individual stars, which are not in phase with the $T_{\rm eff}$ variations. Differences in metallicity and C/O ratios are likely to contribute to the dispersion. Fig. 5 shows the indices most tightly correlated with 710−888. The 200−220 index which is a measure of the strength of H_2O at 2.0 μm relative to the continuum point at 2.2 μm reveals a more pronounced scatter than the VO index when plotted against the $T_{\rm eff}$ indicator 710−888. The 200 and 220 filters are displayed on Fig. 3.

The broad-band colour V−K is not a pure near-infrared index. It is a very good effective temperature index for static cool stars, not so much affected by metallicity effects according to Bessell et al. (1998), and we find it very well correlated with the 710−888 index. V−K values have been computed after extrapolating each observed spectrum (which begins at 5100 Å and ends at 24900 Å) on the blue and on the red sides by the synthetic spectrum which gave the best χ^2 fit. The correction is always less than 0.15 mag (mean: 0.09 mag). Bessell et al. (1998) have determined polynomial fits to empirical effective temperature versus V−K relations for giants. Fig. 6 shows the comparison between the effective temperature obtained using their relation (their Table 7, data sets 'abcd') and the static $T_{\rm eff}$ we determined in Sect. 3.2: the agreement is good. The broad-band colours I−J and I−K are almost as good $T_{\rm eff}$ indicators as V−K (Fig. 5). A systematic difference between the supergiants (triangles) and the other stars is seen: their I−J and I−K tend to be larger at given 710−888.

4. Bolometric corrections

The large spectral region covered by the observations and the fact that the cool stars emit most of their energy in the near-infrared enable us to compute bolometric corrections. A first order correction to the determination of the bolometric luminosity has been applied by extrapolating the observed energy distributions on the blue and red sides by synthetic spectra as explained in Sect. 3.3.2. The mean correction on the bolometric magnitudes amounts to 0.22 mag. No additional correction was added in the case of dust shell enshrouded stars (see Sect. 5). The zero-point of the bolometric scale is computed with the following values (Bessell et al. 1998): $M_{\rm bol,\odot}$=4.74, $M_{\rm V,\odot}$=4.81, $V_\odot$=−26.76, $f_{\rm tot,\odot}$=1.371×10^6 erg cm^{-2} s^{-1}. The absolute flux at 5556 Å of the Vega model is set to 3.44 10^{-9} erg cm^{-2} s^{-1} Å^{-1} (Hayes 1985) to achieve a V magnitude of 0.03 mag for Vega (Bessell et al. 1998). Fig. 7 presents the bolometric correction $BC_{\rm I} = m_{\rm bol} - I$ versus I−J. This relation is of particular interest for the ongoing infrared sky surveys like DENIS (Epchtein 1998). It is remarkable that local, Bulge and LMC/SMC stars, and all variability types follow the very same relation: there is a single narrow sequence for oxygen-rich stars. A polynomial fit gives:

$$m_{\rm bol} - I = 1.32–0.574 \times (I - J) - 0.0646 \times (I - J)^2 \qquad (2)$$

The standard deviation of the relation is 0.09 mag.

A complete study of the bolometric corrections derived from this sample will be presented elsewhere (Mouhcine et al., in preparation).

5. Extinction

The colour indices used in this paper have not been corrected for extinction. To what extent may interstellar and circumstellar matter bias the two-colour relations and add to their dispersion?

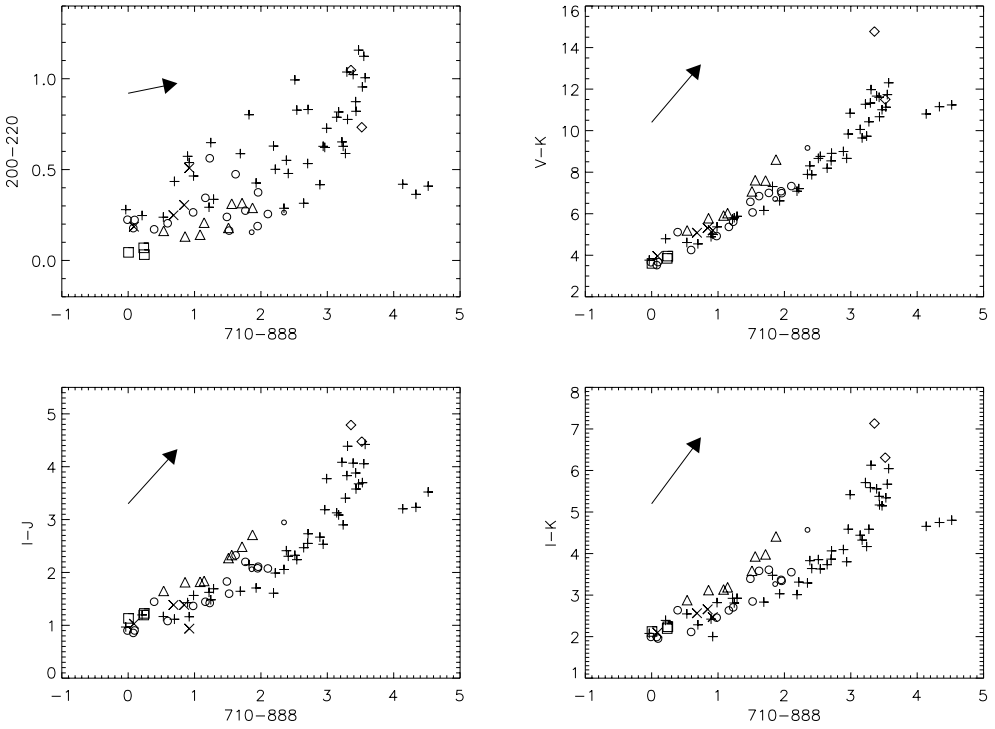

Fig. 5. The 200−220, V−K, I−J and I−K indices versus the temperature indicator 710−888. The arrows give the extinction vectors for an E_{B-V} equal to 1 (see Sect. 5). Same symbols as Fig. 4

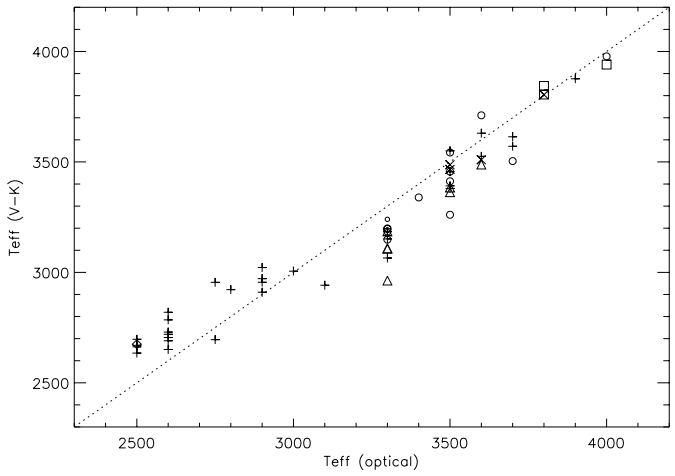

Fig. 6. The effective temperature obtained from V−K and the relation of Bessell et al. (1998) against our static $T_{\rm eff}$ assignment derived from the fit of MARCS models to the optical spectrum (see Sect. 3.2). The dotted line is the one-to-one line. Same symbols as Fig. 4

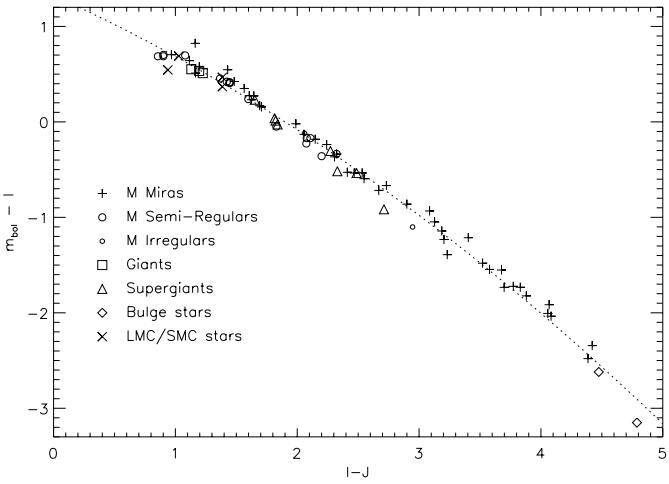

Fig. 7. The bolometric correction $BC_{\rm I}$ as a function of the I−J colour for cool oxygen-rich stars. The dotted line is the polynomial fit

In order to estimate the effects of interstellar extinction on the colours, we used the extended mean extinction law given by Fluks et al. (1994) based on the observed mean extinction law of Savage & Mathis (1979) and on the theoretical extinction law of Steenman & Thé (1989, 1991). From the tabulated $R(\lambda) = a(\lambda)/E_{B-V}$ values, we compute the interstellar extinction correction for band B_i as a function of E_{B-V}:

$$B_i - B_{i,0} = -2.5 \log \frac{\int_0^\infty S_i(\lambda) F(\lambda) d\lambda}{\int_0^\infty S_i(\lambda) F(\lambda) 10^{0.4 R(\lambda) E_{B-V}} d\lambda} \quad (3)$$

where B_i is the uncorrected index, $B_{i,0}$ is the dereddened index, $S_i(\lambda)$ is the response function within the band B_i and $F(\lambda)$ is the observed spectrum. As an approximation, we take $F(\lambda)$ as the arithmetic mean of all the spectra.

To first order, reddening mimics a shift towards lower temperatures in all the usual broad band two-colour plots (e.g. Fig. 5). But molecular band indices may be little affected or even vary orthogonally to the temperature sequence, depending on the separation between the two photometric passbands used, and on the side of the molecular absorption feature on which the "continuum" is measured. Thus, the effect of dust is expected to be most obvious in plots that combine a broad band colour and a molecular index. An example is given in Fig. 8. Most of

the local Miras are grouped along a sequence at J−H $\simeq$ 0.85. The dispersion across the sequence is real, i.e. much larger than observational errors. But only a small fraction of the dispersion may be associated with interstellar extinction: the motion of individual stars in J−H during their pulsation cycle is comparable with the width of the sequence (see the example of the M3 Mira X Men on Fig. 8), while the effect of typical values of the optical depth towards local stars is much smaller (comparable in amplitude to the observational uncertainties). This justifies neglecting interstellar extinction towards local stars.

Two local Miras with very large J−H values (larger than 1.5) are identified in Fig. 8. IO Vir, a M6 Mira, was observed twice. It is a known OH maser (OH 334.7+50.0, Turner 1979). This star is thus enshrouded in an important dust shell. So is the second extreme Mira, WX Psc (OH 128.6-50.1). IO Vir and WX Psc are the only two Miras of our sample with an OH designation: this corroborates the fact that circumstellar matter, as opposed to interstellar matter, is responsible for their red colours. Infrared excess is measured by the ratio F(12 μm)/F(2.2 μm) (see Habing 1996 and references therein; Le Bertre & Winters 1998). This ratio has been derived from the IRAS PSC (IRAS Science Team 1988) and from the K magnitude (Gezari et al. 1996), whenever available (using the calibration of Beckwith et al. (1976) to convert K magnitudes into fluxes at 2.2 μm). As expected, Fig. 9 clearly shows that WX Psc and IO Vir (and to some extent IRC −20427) have large F(12 μm)/F(2.2 μm) ratio. The presence of cool circumstellar material around these stars is thus confirmed and explains their large J−H colours.

Even in the extremely obscured cases mentioned above, the data do not indicate a significant contribution of circumstellar continuum emission at wavelengths shorter than 2.4 μm. Such a warm dust contribution would reduce the equivalent widths of the CO bands (Tanaka et al. 1996). No significant reduction is observed in our essentially O-rich sample. The depths and shapes of the CO bands ($\lambda \geq 2.29$ μm) of the naturally reddened spectra compare very well to those of cool unobscured Miras like X Men, once the latter have been artificially reddened to match the colours of the former.

The Bulge stars systematically lie above the sequence of local optical LPVs. The interstellar extinction effect is obvious. The extinction towards the Sgr I and NGC 6522 galactic Bulge fields, to which the Bulge stars of our sample belong, corresponds to $E_{B-V} \simeq 0.55$ according to estimates in the literature (Wood & Bessell 1983; Glass et al. 1995; Barbuy et al. 1998). Once corrected for reddening, the observed Bulge stars lie on the edge of the local Mira sequence. This is consistent with the fact that, for Bulge stars, a large J−K index has been used as a selection criterion for inclusion in the spectroscopic sample. However, the spectra indicate that at least some of the observed Bulge stars are reddened more than the average Sgr I and NGC 6522 field stars: for instance, the spectrum of Sgr I N°11 (observed in July 1996) is very well matched, in terms of the energy distribution, the molecular bands and the global aspect of metal line blends, by the spectrum of the local Mira RS Hya (February 1995) if $E_{B-V} = 1$. An equally good match is obtained between the local X Men (March 1996) and NGC 6522 N°435 (May 1996) with $E_{B-V} = 1.6$. This additional extinction may be due in various proportions to circumstellar matter and to the patchy distribution of interstellar dust. Similarly high extinction values are found towards various star clusters in the neighbourhood of the Galactic Centre (Barbuy et al. 1998). Only two of the Bulge stars of the sample have been detected by IRAS (NGC 6522 N°435= IRAS 17593-3006, NGC 6522 N°205=IRAS 17591-2959; Glass 1986; Glass et al. 1995). Using the K magnitudes of Wood & Bessell (1983), we obtain 12 μm to 2.2 μm flux ratios of 1.05 and 1.6, respectively, i.e. relatively low values as compared to the local IRAS sources of Fig. 9. Again, the strong CO absorption longward of 2.29 μm argues against a significant contribution of warm circumstellar dust emission to the near-IR light of the Bulge LPVs.

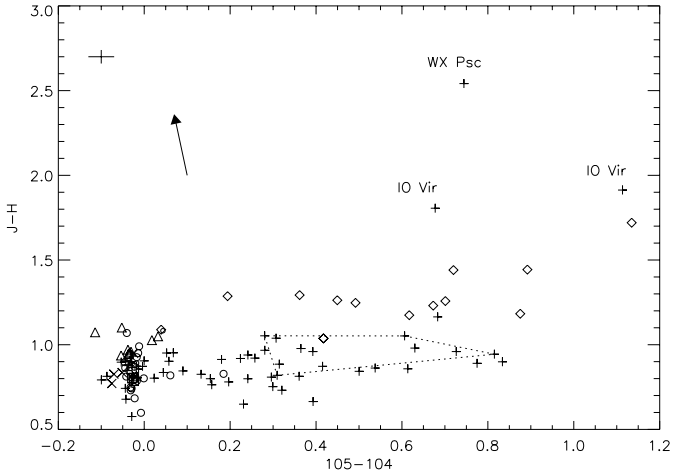

Fig. 8. J−H versus the near-infrared $T_{\rm eff}$ indicator 105−104. The arrow gives the extinction vector for an E_{B-V} equal to 1. The cross in the upper left corner gives the typical error bars. Lines connect observations of X Men, an M3 Mira, at various phases. Same symbols as Fig. 4

The Bulge stars tend to display strong VO and TiO bands; molecular bands need to be observed in a larger unbiased sample in order to determine whether this is or is not due to the selection of red and luminous objects.

6. Water in Long Period Variable stars

The most distinctive features in the near-IR spectra of pulsating red giants are their impressive H_2O absorption bands. Johnson & Méndez (1970) already observed Mira type LPVs with much deeper water vapour bands than static giants of similar spectral types. LPV models (Bessell et al. 1989b; Bessell et al. 1996) and observations (e.g. Matsuura et al. 1999) have subsequently confirmed that deep H_2O features are related to pulsation and have provided basic understanding: pulsation produces much more extended atmospheres, and in addition dense cool layers may result from the periodical outwards running shocks. In various ways pulsation thus leads to the existence of regions where relatively low temperatures ($\sim 10^3$ K or lower) are combined with relatively high densities, conditions that favour the formation of H_2O and possibly even of dust (Bowen 1988; Feuchtinger et al. 1993; Jeong et al. 1999).

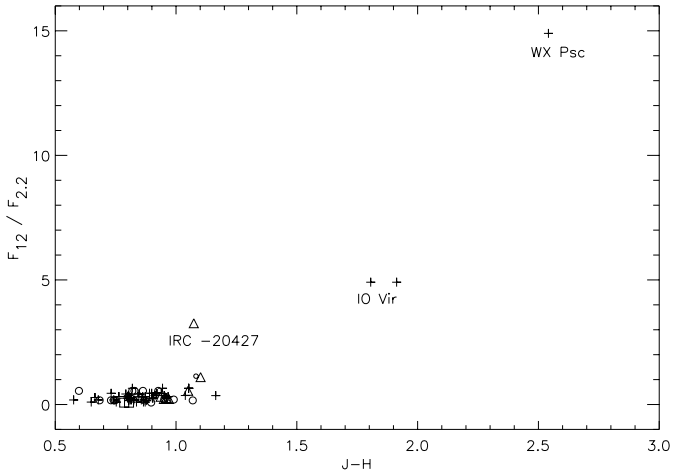

Fig. 9. The F(12 μm)/F(2.2 μm) ratio versus J−H. Three stars (WX Psc, IO Vir and IRC −20427) present an infrared excess due to the presence of a cool circumstellar shell. Same symbols as Fig. 4

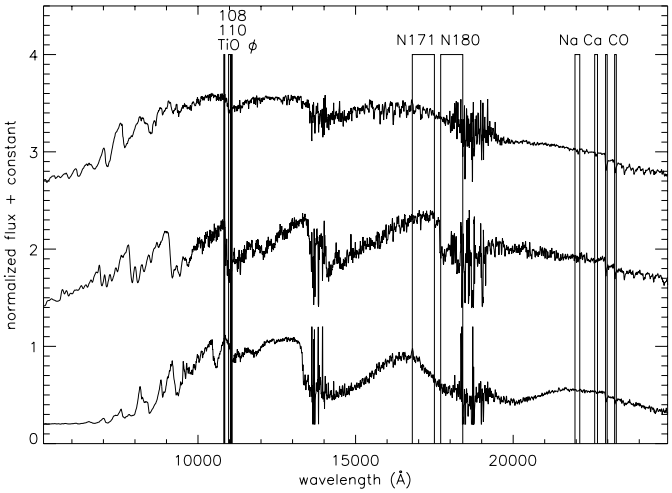

Fig. 10. Filters used in Sect. 7. Same spectra as Fig. 3

Fig. 5 (top left) shows that H_2O absorption indices for LPVs range from 0 to values far above those the coolest static giants reach. At a given stellar energy distribution a large range of H_2O absorption indices is found (a similar phenomenon has been described for SiO bands by Aringer et al. 1999). Even relatively warm LPV spectra (instantaneous $T_{\rm eff} \geq 3500$ K) may display deep water vapour bands, a behaviour that remains to be reproduced quantitatively by LPV models (Mouhcine & Lançon 1998). More data (in particular complete phase coverage for more stars) is required to gain better insight into the relation between the H_2O features, pulsation amplitude, phase, metallicity and details of the stellar structure.

For the purposes of this paper, we conclude that deep H_2O features can be taken as a clear indication for pulsation, while the absence of water vapour does not exclude that the observed star be an LPV.

7. Supergiants, giants and variability types

From a spectrophotometric point of view, supergiants, giants and dwarfs are usually separated mainly on the basis of CO and H_2O absorption, which respectively strengthens and weakens from luminosity class V to I (e.g. Aaronson et al. 1978; Kleinmann & Hall 1986; Origlia et al. 1993). The strength of various metal lines, e.g. the Na doublet at 2.20 μm and the Ca triplet at 2.26 μm, also depend on the luminosity class. Ramírez et al. (1997) found that the quantity log[EW(CO)/(EW(Na) + EW(Ca))] is an excellent luminosity indicator, at least for K and M giants and dwarfs. Bessell et al. (1989a) identified the CN band at 1.1 μm as a surface gravity sensitive feature.

In this section, we summarise the results of a systematic search for indices that separate the giants from supergiants of our sample. Our sample contains 10 supergiant observations: 3 non-variable supergiants, plus 3 Semi-Regular variables of the SRc type, plus 3 Irregular variables of the Lc type, one of them observed twice. All these supergiants are of spectral type M0 or later. The sample stars being cooler than those of Ramírez et al. (1997) and our spectral resolution lower, the CaI and NaI features around 2.2 μm are seriously blended with molecular absorption features, leading us to redefine Na and Ca indices. The passbands and indices used are defined in Table 1. The passbands for CO measurements around 2.3 μm are taken from Kleinmann & Hall (1986). F180W and F171W correspond to the Hubble Space Telescope narrow band NICMOS filters. They were initially designed to measure the strength of the 1.7 μm C_2 absorption band in carbon stars (Thompson, private communication), but actually provide a good H_2O absorption index (see Lançon et al. 1999 for applications to stellar population studies). Other common H_2O indices (e.g. based on Wing filters at 2.0 and 2.2 μm) would lead to qualitatively similar results. The selected filters are displayed on Fig. 10.

Table 1. Filters used to define indices liable to separate giants and Miras from supergiants

Filter name	Center (Å)	Width (Å)	Comments
F171W	17150	700	HST NICMOS band
F180W	18050	700	HST NICMOS band, $H_2O + C_2$
$xNac_1$	21920	20	'continuum' # 1 for Na
$xNac_2$	21960	20	'continuum' # 2 for Na
xNa	22036	152	Na I doublet
$xNac_3$	22120	20	'continuum' # 3 for Na
$xNac_4$	22168	25	'continuum' # 4 for Na
$xCac_1$	22548	75	'continuum' # 1 for Ca
xCa	22630	90	Ca I triplet
$xCac_2$	22703	55	'continuum' # 2 for Ca
xCOc	22899	52	'continuum' for CO
xCO_1	22957	52	^{12}CO(2,0) band-head
xCO_2	23245	54	^{12}CO(3,1) band-head

$CO = -2.5\ \log[(xCO_1+xCO_2)/xCOc] - CO(Vega)$
$Na = -2.5\ \log[xNa/(xNac_1 + \ldots + xNac_4)] - Na(Vega)$
$Ca = -2.5\ \log[xCa/(xCac_1+xCac_2)] - Ca(Vega)$
$H_2O = -2.5\ \log[F180W/F171W] - H_2O(Vega)$

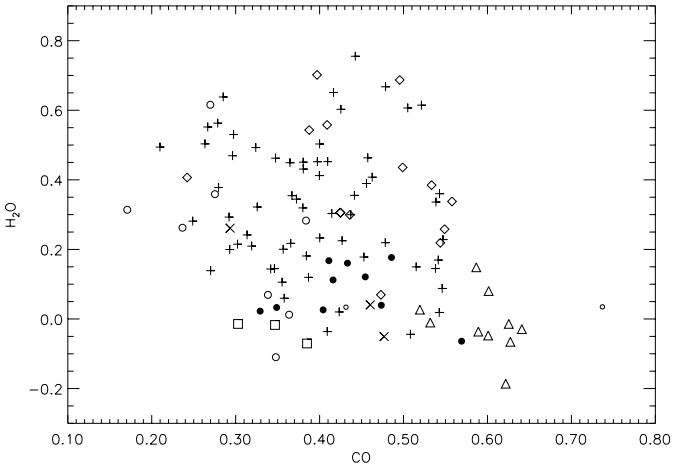

Fig. 11. The H_2O index versus the CO index (see Sect. 7). Same symbols as Fig. 4 except for M Semi-Regulars (empty circles: SRa; filled circles: SRb). Supergiants (triangles) are discriminated in this diagram

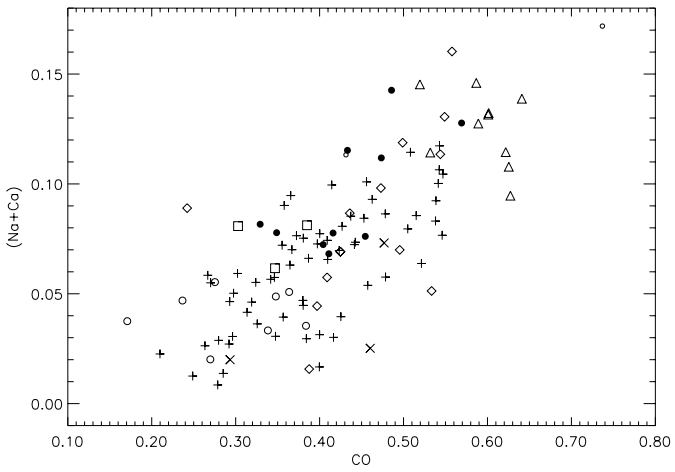

Fig. 12. The (Na+Ca) index versus the CO index (see Sect. 7). Same symbols as Fig. 11

The CO, H_2O and metal line measurements are plotted in Fig(s). 11 and 12. Supergiants systematically provide the highest metal line and CO indices of the sample of O-rich stars (carbon stars are discussed in Sect. 8). As expected, their mean CO and metal absorption is high and their mean H_2O absorption low, compared to the mean properties of the M type variable giants of luminosity class III. The combined constraints CO ≥ 0.51, H_2O ≤ 0.15 and (Na+Ca) ≥ 0.09 isolate the supergiants with only 3 intruders: one of the two observations of KV Car (SRb variable), one of the three observations of WW Sco (Mira variable) and the observation of V774 Sgr (Lb variable).

The luminosity class sensitivity of the CO/(Na+Ca) combination of Ramírez et al. (1997) indeed extends to giant and supergiant luminosities. However, since (at a resolution of 1100) the centers of the Na and Ca line blends lie typically 10 % below the so-called continuum and their range of variation is small compared to the range of variation of CO absorption, the combined index carries information similar to the CO index itself.

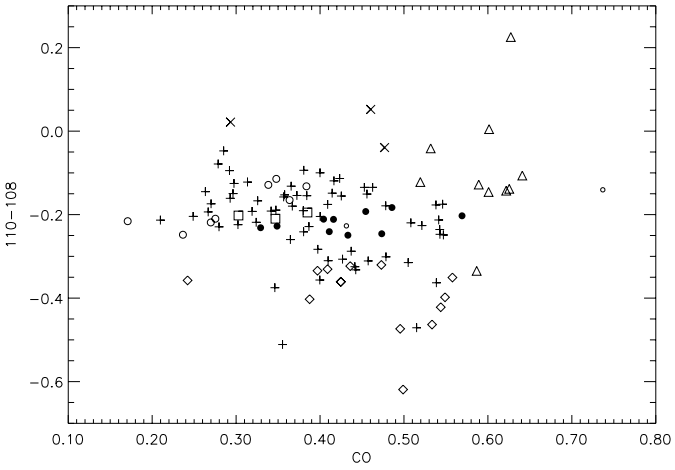

Fig. 13. The CN absorption index 110−108 versus the CO index. Same symbols as Fig. 11

The isolation of the supergiants appears particularly clearly when a CO measurement is combined with the gravity indicator of Bessell et al. (1989a), the CN index 110-108 (Fig. 13). In the same way, TiO indices measuring the ϕ bands at 1.1 or 1.2 μm are absent in supergiants, and provide an alternative segregation tool (Fig. 14). These TiO indices are useful to identify very cool AGB stars. The 108, 110 and TiO ϕ filters are shown in Fig. 10.

Figs. 11–14 also indicate a tendency for SRa type LPVs to have a lower CO index than SRb type variables. According to Kerschbaum & Hron (1992, 1994), SRa type variables appear as intermediate objects between Miras and SRb variables in several aspects. This assertion seems supported by Fig(s). 11–14 concerning the CO absorption band. We note nevertheless that only 2 SRa variables (adding up to 8 observations) and 4 SRb variables (10 observations) have been observed. More spectroscopic data should be studied to confirm this effect.

8. Chemical types

The spectra of carbon stars have little in common with those of oxygen-rich giants appart from CO absorption and a red energy distribution (Fig. 10). While, according to both observations and model atmospheres, it might be possible to identify selected regions of the near-IR spectra of O-rich LPVs as quasi-continuum windows (e.g. 1.04 μm, 2.15 μm), the whole optical and near-IR range of C-rich stars is shaped by molecular bands of carbon based molecules. In the wavelength range under consideration the C-rich spectra display much less temperature and pulsation phase dependence than O-rich spectra.

Our sample includes 26 NIR spectra of 6 carbon-rich stars. Four are Semi-Regular LPVs (7 spectra of RU Pup, 6 of Y Hya, 3 of T Cae, 1 of S Cen). The two Mira-type variables are the dust-enshrouded R Lep and the SC star BH Cru. Although the sample may not be representative of all C-rich stars, it allows us to demonstrate which spectrophotometric indices are useful in the separation of chemical subtypes.

It is well known that stars can be to a certain point separated into carbon stars and oxygen stars using broad band colour–

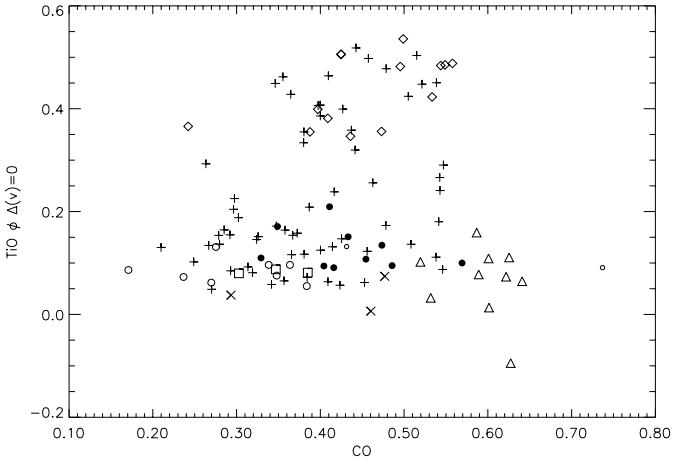

Fig. 14. The absorption index of TiO ϕ (Δv=0) versus the CO index. Same symbols as Fig. 11

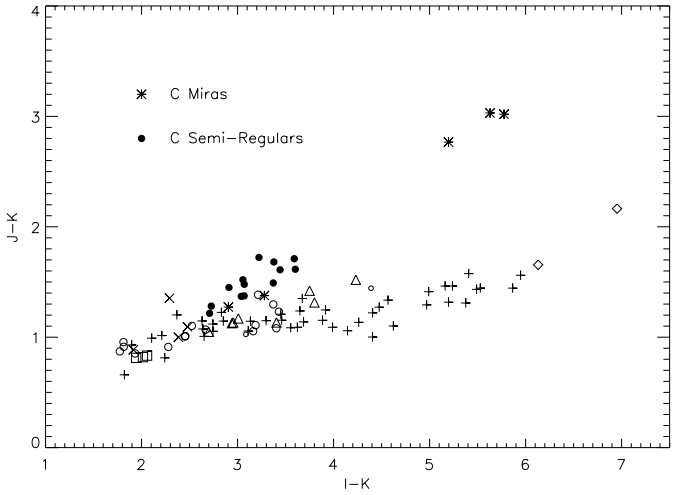

Fig. 15. J−K versus I−K. Carbon-rich Miras are represented by asterisks and carbon-rich Semi-Regulars by filled circles. Otherwise, same symbols as Fig. 4

colour diagrams (e.g. Frogel et al. 1980, 1990; Feast 1994; Zijlstra et al. 1996; Loup et al. 1998). C-rich stars appear in general redder than O-rich stars in such diagrams, and as a consequence, an often heard statement is that carbon stars are the reddest giants.

The present data shows that this is not in general true. It is based on Magellanic Cloud data and is likely to hold for metal-deficient environments, where few if any very cool O-rich AGB stars are expected to exist because dredge-up of carbon produces C-stars more efficiently, but it must be reconsidered in the solar neighbourhood or in more general surveys. Excluding objects of our sample for which the presence of a circumstellar envelope is known, the O-rich LPV sequence reaches much redder values than the C-rich sequence in most colours (e.g. V−I, V−K, R−K, I−K). The colour distribution is similar for both chemical types in H−K.

Most pure optical/NIR colours are thus insufficient to enable an unambiguous discrimination if used alone, and colours strongly affected by the specific molecular features of carbon stars are needed. Zijlstra et al. (1996) suggest the infrared colour K−[12], in which C-stars appear relatively red due to HCN and possibly C_2H_2 absorption in the 12–14μm range (Hron et al. 1998). J−K also is a useful indicator. Due to CN and C_2 absorption in the J band, the C-stars appear systematically redder in this colour than O-rich stars with, for instance, identical I−K values (Fig. 15). J−K $\geq$ 1.5 or 1.6 has been used for the separation of C-stars in LMC surveys (Loup et al. 1998; Wood et al. 1999). O-rich spectra with higher J−K values exist among the stars with no obvious dust shells of our sample, but they are rare. They generally correspond to Mira-type variables observed at minimum light. The J−K criterion remains applicable at solar metallicities, but it misses the warmer of the C-stars and only holds if M-stars with strong mass loss (and circumstellar emission) have previously been excluded. The narrow-band molecular indices discussed below avoid confusion.

The most obvious features identifying C-star spectra are those of CN and C_2 bands. Indices for CN measurements include the Wing pairs 110−108 or 110−123, as well as the more selective narrow band index based on the first 2 filters in Table 2. Indices sensitive to the steep Ballik-Ramsay C_2 bandhead at 1.77 μm (Ballik & Ramsay 1963; Goorvitch 1990) include the HST NICMOS intermediate band index F180W−F171W and the narrow band index based on the nearly adjacent last 2 filters in Table 2. The filters are shown in Fig. 16.

Table 2. Filters used to define indices which measure carbon species

Filter name	Center (Å)	Width (Å)	Comments
xCN_{cont}	10840	30	'continuum' for CN
xCN	10885	40	CN A–X Δv=0 transition
$xC_{2,cont}$	17570	100	'continuum' for C_2
xC_2	17750	140	Ballik-Ramsay band

In Fig. 17, the NICMOS index F180W−F171W is plotted against the narrow band C_2 index. The good correlation among each sequence comes from the overlap between the passbands used for both indices. However, only in the narrow band index are the two filters close enough not to be sensitive to the broad absorption band of H_2O. While the NICMOS colour is able to identify LPVs independently of their chemical type, it is not capable of separating C-rich objects from O-rich ones (Lançon et al. 1999).

Fig. 18 shows the CN index against the C_2 index. Once again, the oxygen-rich stars are clearly separated from carbon-rich stars as expected. The O-rich stars are now grouped together instead of forming a sequence.

Another noticeable feature in Fig(s). 17 and 18 is the apparent segregation between carbon Miras and carbon Semi-Regular variables. If, on average, Mira-type pulsation is reached at a later evolutionary stage on the AGB than Semi-Regular pulsation, as suggested by recent studies of period–luminosity sequences in the LMC (Wood et al. 1999), and if the C_2 band strength depends primarily on the C/O ratio, which on average increases with time along the AGB, then one expects to find the C-rich

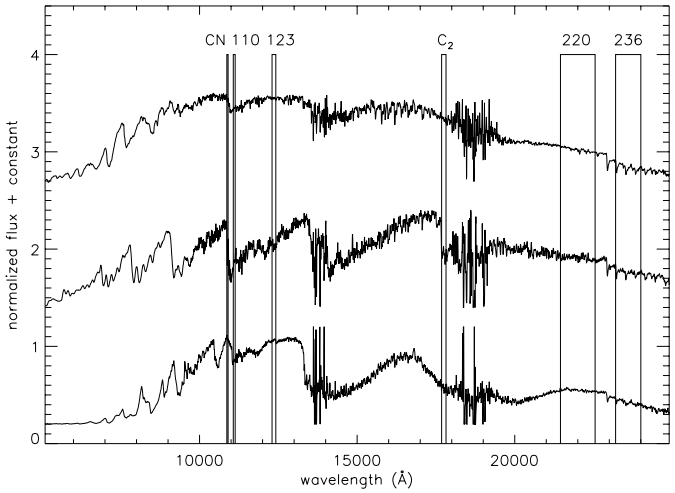

Fig. 16. Filters used in Sect. 8. Same spectra as Fig. 3

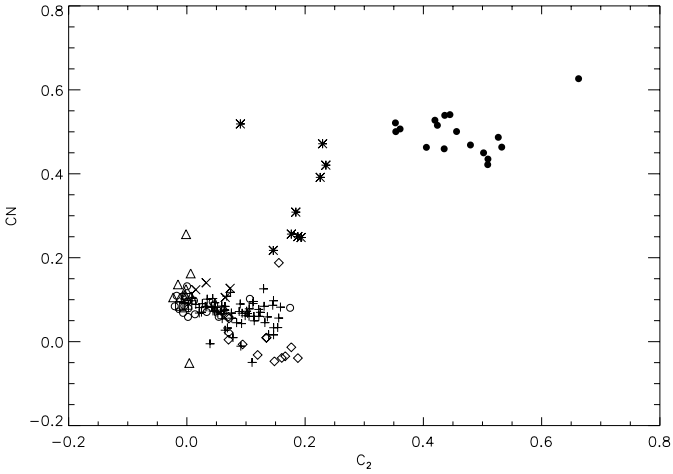

Fig. 18. The CN index versus the C_2 index. Same symbols as Fig. 4 and Fig. 15

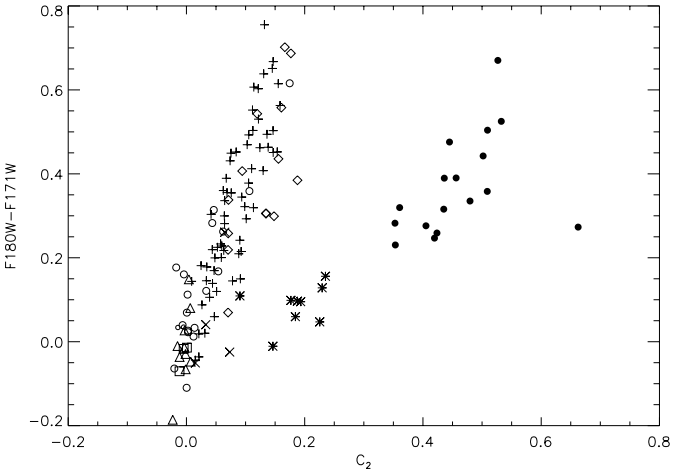

Fig. 17. The NICMOS index F180W−F171W versus the C_2 index. Same symbols as Fig. 4 and Fig. 15

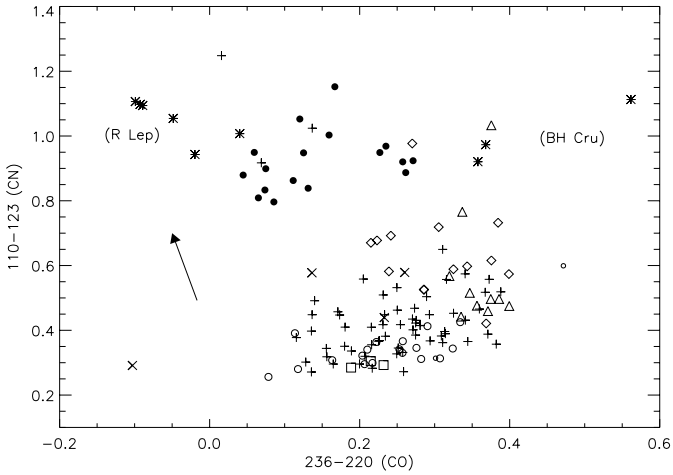

Fig. 19. The 110−123 index versus the 236−220 index. Same symbols as Fig. 4 and Fig. 15. The six observations of the C-Mira R Lep and the three observations of the SC-Mira BH Cru are indicated. The arrow gives the extinction vector for an E_{B-V} equal to 1

Miras at higher C_2 indices than the Semi-Regulars. This simple global scenario cannot be applied to samples as small as this one. In particular, the SC star BH Cru pulsates like a Mira variable although its C/O ratio is close to 1. Larger and more representative samples are required to study systematic effects of the pulsation type.

The CO indices measured for carbon stars cover the full range observed for O-rich objects, including supergiant stars. In particular, the 2.3 μm CO absorption of the SC star BH Cru compares to the strongest band observed in our supergiant sample. This must be taken as a warning against the exclusive use of the CO index in searches for red supergiant stars (although the rarity of SC type stars prevents this finding from being of major concern in the study of integrated spectra of stellar populations).

As already mentioned in the case of C_2, the comparison of the CO index defined in Sect. 7 with the larger baseline index 236−220 illustrates the advantages of using narrow filters located very close to the feature of interest (Fig. 19): the extremely low 236−220 index of R Lep is merely due to its extremely red energy distribution; the systematic shift in CO between the 236−220 values of C-rich and O-rich stars is explained by additional molecular absorption in the 220 band; the shift in both CO and CN between Bulge and solar neighbourhood objects is mainly the effect of extinction. Colour corrections are required to circumvent ambiguities in the large baseline indices (Frogel & Whitford 1987).

9. $^{12}C/^{13}C$ ratio

The $^{12}C/^{13}C$ ratio in red giants is an important indicator of nuclear processing that occurs inside a star. The first dredge-up occurs when the star ascends the first giant branch: the number ratio $^{12}C/^{13}C$ drops from its initial value of ~ 90 to between 18 and 26 (Charbonnel 1994). The intermediate-mass stars ($\geq$ 3–4 $\mathcal{M}_\odot$) undergo a second dredge-up at the beginning of the AGB: the $^{12}C/^{13}C$ ratio decreases a little bit more for these stars. Then, the $^{12}C/^{13}C$ ratio increases along

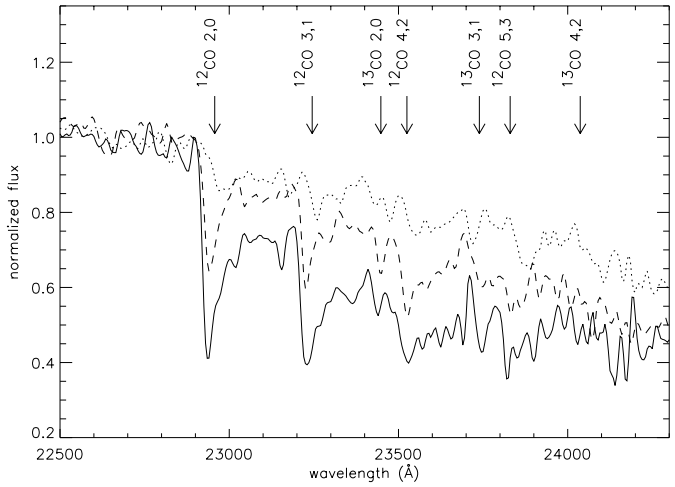

Fig. 20. Spectra exhibiting ^{12}CO and ^{13}CO lines with decreasing strength (solid line: BH Cru, an SC Mira; dashed line: RS Hya, an M Mira; dotted line: S Car, an M Mira)

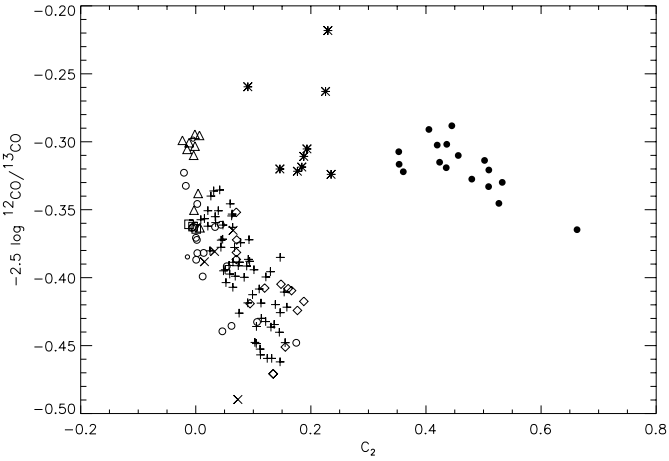

Fig. 21. The ^{12}CO/^{13}CO index as a function of the C_2 index. Same symbols as Fig. 4 and Fig. 15

the Thermally-Pulsating Asymptotic Giant Branch as the third dredge-up enriches the stellar surface with freshly synthesized elements (e.g. Forestini & Charbonnel 1997). However, when Hot Bottom Burning occurs, this ratio drops again to small values (Boothroyd et al. 1993). The ^{12}C/^{13}C isotope ratio is thus likely to exhibit a large spread of values for a given sample of cool giants. Our set of spectra enables us to check for an evolution of the ^{12}C/^{13}C ratio.

Fig. 20 shows three examples of star which exhibit ^{12}CO and ^{13}CO lines with decreasing strength (solid line: SC4.5–SC7 Mira BH Cru; dashed line: M6 Mira RS Hya; dotted line: K5–M6 Mira S Car). Positions of the CO bandheads are shown. The spectra are normalized to a common flux (F_λ) around 22 900 Å.

A semi-quantitative approach using photometric indices is illustrated in Fig. 21. A ^{12}CO/^{13}CO index is computed from the fluxes in rectangular 80 Å wide filters, respectively centered in the four ^{12}CO and the three ^{13}CO bandheads shown in Fig. 20. It is expected to vary with the ^{12}C/^{13}C ratio. It is plotted in Fig. 21 against the C_2 index (Table 2) which separates C-rich from O-rich stars. Interstellar extinction has a negligible effect on the indices of Fig. 21.

The C-rich stars exhibit the larger ^{12}CO/^{13}CO indices: as expected, the ^{12}C/^{13}C ratio increases as the star undergoes third dredge-up that turns it into a carbon star. Supergiants (triangles) have also large ^{12}CO/^{13}CO indices compared to giants and LPVs. It may not be due to intrinsic large values of ^{12}C/^{13}C. Indeed, predicted ^{12}C/^{13}C ratios from computations are weakly dependent on stellar mass at $\mathcal{M} \geq 2\,\mathcal{M}_\odot$ (El Eid 1994): supergiants are not expected to exhibit large ^{12}C/^{13}C ratios. On the contrary, supergiants have in most cases low observed ^{12}C/^{13}C ratios (α Ori and α Sco for instance, Harris & Lambert 1984). More probably, the large ^{12}CO/^{13}CO are due to radiative transfer effects on the CO bands (luminosity, atmospheric extension, line blends with other species).

Oxygen-rich LPVs exhibit a large spread of ^{12}CO/^{13}CO indices, sometimes with values comparable to C-rich stars. Model atmospheres would be necessary to carefully determine the ^{12}C/^{13}C ratios of our sample stars and explain some of the trends in Fig. 21, and compare to predicted computations from evolutionary models.

10. Conclusion

We have explored the large sample of optical and near-infrared spectra of Lançon & Wood (1998 and in preparation), and derived useful tools to connect spectrophotometric signatures with fundamental properties of cool oxygen- and carbon-rich LPVs and supergiants.

Temperatures of oxygen-rich stars are assigned on the basis of synthetic spectra, computed with up-to-date oxygen-rich model atmosphere grids (Plez 1992; Plez, private communication) and adjusted to the optical data. They range from 2500 K to 4000 K. It is recalled that the relationship between this semi-empirical temperature and effective temperature is expected to depend on pulsation properties as well as on the more usual physical attributes of a star (metallicity, surface gravity). While several optical colours appear to be rather good indicators of the assigned temperature (e.g. 710−888), only a few purely near-infrared temperature indicators were found. The Wing colour 105−104 and the broad-band colours I−J and I−K can be used as a first approximation. The lack of better near-infrared temperature indicators is unfortunate for extragalactic survey purposes. V−K, although not a purely NIR colour (and thus also more sensitive to extinction), proves to be a very convenient indicator of the optically assigned temperature over the whole range exhibited by the sample stars.

The large spectral region covered by the observations enables us to derive a relation between the bolometric correction BC_I and the broad-band colour I−J for oxygen-rich cool stars. The standard deviation is only of 0.09 mag. It can be applied as a first approximation to red giants, supergiants and LPVs. This relation is of particular interest for ongoing infrared sky surveys.

Interstellar extinction towards most stars of the solar neighbourhood sample appears to be small. Only four local stars (IO Vir, WX Psc, R Lep and IRC −20427) are clearly dust enshrouded. Even the latter display deep CO bands at 2.3 μm, arguing against a significant contamination by circumstellar dust emission in the near-IR.

Deep H_2O features present in the near-IR spectra are a strong indication of pulsation. Nevertheless, the absence of water vapour does not exclude that the observed star is an LPV.

Luminosity class I stars can be efficiently distinguished from luminosity class III stars with appropriate combinations of indices based on CO, H_2O, Na, Ca, CN or TiO lines. SRa type LPVs show a tendency for lower CO indices than SRb variables.

In order to separate carbon-rich LPVs from oxygen-rich stars, colours strongly affected by the specific molecular features of carbon stars are needed. Selected broad-band colours (e.g. J−K) are useful indicators, but narrow-band molecular indices based on CN and C_2 bands are by far more efficient.

A $^{12}CO/^{13}CO$ index has been computed from the empirical spectra. As expected if the $^{12}CO/^{13}CO$ index actually varies with the $^{12}C/^{13}C$ ratio, the C-rich stars exhibit on average larger index values than the O-rich stars. The supergiants of the sample also exhibit large $^{12}CO/^{13}CO$ indices. This behaviour is opposite to what is expected from evolution models. This might be due to radiative transfer effects on the CO bands (luminosity, atmospheric extension, line blends with other species).

The different indices and relations discussed are useful in the interpretation of integrated NIR spectra of stellar populations and of the considerable amount of data provided by ongoing infrared sky surveys, as well as in infering stellar properties of individual cool giants and supergiants. However, in order to resolve remaining ambiguities and to gain quantitative information, the dependence of the observable indices on stellar parameters, surface abundances, environement, etc, must be more extensively investigated. Only comparisons to models will eventually permit to complete this work. Extreme difficulties result from the fact that many complex aspects of LPV modelling (oxygen-rich/carbon-rich transition, pulsational distinction between Mira and Semi-Regular variables, effects of pulsation on the atmosphere, non-grey emergent spectra, etc.) should be taken into account simultaneously. Some recent and important progress allows us to hope that this formidable task might be carried out in a future not completely out of reach.

Acknowledgements. RA gratefully thanks D. Egret and J-L. Halbwachs for their hospitality and for providing financial support while he was staying at the Strasbourg Observatory. RA benefits of a EU TMR "Marie Curie" Fellowship at ULB. Part of this work was completed while BP was at Uppsala Astronomiska observatoriet and at the Atomspektroskopi division in Lund. B. Gustafsson and S. Johansson are both thanked for their support and hospitality. This research has made use of the Simbad database operated at CDS, Strasbourg, France.

References

Aaronson M., Persson S.E., Frogel J.A., 1978, ApJ 220, 442
Alvarez R., Mennessier M-O., 1997, A&A 317, 761
Alvarez R., Plez B., 1998, A&A 330, 1109
Aringer B., Höfner S., Wiedemann G., et al., 1999, A&A 342, 799
Ballik E.A., Ramsay D.A., 1963, ApJ 137, 61
Barbuy B., Bica E., Ortolani S., 1998, A&A 333, 117
Baschek B., Scholz M., Wehrse R., 1991, A&A 246, 374
Beckwith S., Evans N.J., Becklin E.E., Neugebauer G., 1976, ApJ 208, 390
van Belle G.T., Dyck H.M, Benson J.A, Lacasse M.G., 1996, AJ 112, 2147
Bessell M.S., 1990, A&AS 83, 357
Bessell M.S., Brett J.M., 1988, PASP 100, 1143
Bessell M.S., Brett J.M., Wood P.R., Scholz M., 1989a, A&AS 77, 1
Bessell M.S., Brett J.M., Wood P.R., Scholz M., 1989b, A&A 213, 209
Bessell M.S., Scholz M., Wood P.R., 1996, A&A 307, 481
Bessell M.S., Castelli F., Plez B., 1998, A&A 333, 231
Boothroyd A.I., Sackmann I.J., Ahern S.C., 1993, ApJ 416, 762
Bowen G.H., 1988, ApJ 329, 299
Brett J.M., 1990, A&A 231, 440
Bruzual G.A., Charlot S., 1993, ApJ 405, 538
Castelli F., Kurucz R.L., 1994, A&A 281, 817
Charbonnel C., 1994, A&A 282, 811
El Eid M.F., 1994, A&A 285, 915
Epchtein N., 1998. *The Deep Near Infrared Survey of the Southern sky (DENIS).* In: N. Epchtein (ed.) The Impact of Near-Infrared Surveys on Galactic and Extragalactic Astronomy, Kluwer, Dordrecht, p. 3
Feast M., 1994, Ap&SS 217, 117
Feuchtinger M.U., Dorfi E.A., Höfner S., 1993, A&A 273, 513
Fleischer A.J., Gauger A., Sedlmayr E., 1992, A&A 266, 321
Fluks M.A., Plez B., Thé P.S. et al., 1994, A&AS 105, 311
Forestini M., Charbonnel C., 1997, A&AS 123, 241
Frogel J.A., Whitford A.E., 1987, ApJ 320, 199
Frogel J.A., Persson S.E., Cohen J.G., 1980, ApJ 239, 495
Frogel J.A., Mould J., Blanco V.M., 1990, ApJ 352, 96
Gezari D.Y., Pitts P.S., Schmitz M., Mead J.M., 1996, *Catalog of Infrared Observations* (edition 3.5), unpublished, available from VizieR (CDS, Strasbourg)
Glass I.S., 1986, MNRAS 221, 879
Glass I.S., Whitelock P., Catchpole R.M., Feast M.W., 1995, MNRAS 273, 383
Goorvitch D., 1990, ApJS 74, 769
Habing H.J., 1996, A&AR 7, 97
Haniff C.A, Scholz M., Tuthill P.G., 1995, MNRAS 276, 640
Harris M.J., Lambert D.L., 1984, ApJ 281, 739
Hayes D.S., 1985. In: D.S. Hayes, L.E. Pasinetti, A.G. Davis Philip (eds.) Calibration of Fundamental Stellar Quantities (IAU Symp. 111), Reidel, Dordrecht, p. 225
Hofmann K-H., Scholz M., Wood P.R., 1998, A&A 339, 846
Höfner S., 1999. In: T. Le Bertre, A. Lèbre, C. Waelkens (eds.) AGB Stars (IAU Symp. 191), ASP Conf. Ser., p. 159
Höfner S., Jørgensen U.G., Loidl R., Aringer B., 1998, A&A 340, 497
Hron J., Loidl R., Höfner S., et al., 1998, A&A 335, L69
IRAS Science Team, 1988, *IRAS Point Source Catalogue*, prepared by C.A. Beichman, G. Neugebauer, H.J. Habing, P.E. Clegg, T.J. Chester, NASA RP-1190
Jeong K.S., Winters J.M., Sedlmayr E., 1999. In: T. Le Bertre, A. Lèbre, C. Waelkens (eds.) AGB Stars (IAU Symp. 191), ASP Conf. Ser., p. 233
Johnson H.J., Méndez M.E., 1970, AJ 75, 785
Kerschbaum F., Hron J., 1992, A&A 263, 97
Kerschbaum F., Hron J., 1994, A&AS 106, 397

Kerschbaum F., Hron J., 1996, A&A 308, 489
Kholopov P.N., Samus N.N., Frolov M.S. et al., 1988, *General catalogue of Variable Stars*, Fourth Edition, Nauka Publ. House, Moscow
Kleinmann S.G., Hall D.N.B., 1986, ApJS 62, 501
Labeyrie A., Koechlin L., Bonneau D., Blazit A., 1977, ApJ 218, L75
Lançon A., 1999. In: T. Le Bertre, A. Lèbre, C. Waelkens (eds.) AGB Stars (IAU Symp. 191), ASP Conf. Ser., p. 579
Lançon A., Wood P.R., 1998. In: T.R. Bedding (ed.) Fundamental stellar properties: the interaction between observations and theory (IAU Symp. 189), Publ. School of Physics, Univ. of Sidney, p. 168
Lançon A., Mouhcine M., Fioc M., Silva D., 1999, A&A 344, L21
Le Bertre T., Winters J.M., 1998, A&A 334, 173
Loup C., Duc P.A., Fouqué P., Bertin E., Epchtein N., 1998. In: N. Epchtein (ed.) The Impact of Near-Infrared Surveys on Galactic and Extragalactic Astronomy, Kluwer, Dordrecht, p. 115
Matsuura M., Yamamura I., Murakami H., Freund M.M., Tanaka M., 1999, A&A 348, 579
McGregor P., 1994, MSSSO Manual (`http://msowww.anu.edu.au/`)
Mouhcine M., Lançon A., 1998. In: M. Livio (ed.), Unsolved problems in stellar evolution, STScI May Symp., Space Telescope Sc. Inst., Poster Proceedings
Origlia L., Moorwood A.F.M., Oliva E., 1993, A&A 280, 536
Perrin G., Coudé du Foresto V., Ridgway S.T. et al., 1998, A&A 331, 619
Plez B., 1992, A&AS 94, 527
Plez B., 1998, A&A 337, 495
Plez B., 1999a. In: R.F. Wing (ed.) The Carbon Star Phenomenon (IAU Symp. 177), ASP Conf. Ser., in press
Plez B., 1999b. In: T. Le Bertre, A. Lèbre, C. Waelkens (eds.) AGB Stars (IAU Symp. 191), ASP Conf. Ser., p. 75
Plez B., Brett J.M., Nordlund Å, 1992, A&A 256, 551
Ramírez S.V., DePoy D.L., Frogel J.A., Sellgren K., Blum R.D., 1997, AJ 113, 1411
Ridgway S.T., Joyce R.R., White N.M., Wing R.F., 1980, ApJ 235, 126
Savage B.D., Mathis J.S., 1979, ARA&A 17, 73
Scholz M., Takeda Y., 1987, A&A 186, 200
Steenman H.C., Thé P.S., 1989, Ap&SS 159, 189
Steenman H.C., Thé P.S., 1991, Ap&SS 184, 9
Tanaka W., Okada T., Hashimoto O., Yamamura I., Tanabe T., 1996, Publ. Nat. Astron. Obs. Japan 4, 135
Turner B.E., 1979, A&AS 37, 1
White N.M., Wing R.F., 1978, ApJ 222, 209
Wing R.F., 1967, PhD Thesis, University of California, Berkeley
Wing R.F., Alvarez R., Plez B., Yuan Y., 1998. In: T. Le Bertre, A. Lèbre, C. Waelkens (eds.) AGB Stars (IAU Symp. 191), Poster Session, P2–27 (`http://www.dstu.univ-montp2.fr/GRAAL/agb98-1.html`)
Wood P.R., Bessell M.S., 1983, ApJ 265, 748
Wood P.R., Alcock C., Allsman R.A. et al., 1999. In: T. Le Bertre, A. Lèbre, C. Waelkens (eds.) AGB Stars (IAU Symp. 191), ASP Conf. Ser., p. 151
Zijlstra A.A., Loup C., Waters L.B.F.M. et al., 1996, MNRAS 279, 32